Effect of turbulent Mach number on the thermodynamic field generated by a shock wave

By M. S. Yogesh Prasaad AND Krishnendu Sinha

Department of Aerospace Engineering,
Indian Institute of Technology Bombay, Mumbai, 400076

A canonical case of one-dimensional mean flow convecting homogeneous isotropic turbulence across a normal shock wave is studied in this work with special emphasis on the thermodynamic fluctuations generated behind the shock. Direct numerical simulations (DNS) of homogeneous isotropic turbulence interacting with normal shocks of varying strengths have been carried out. Density, pressure and temperature variances attain large values at the shock, followed by, in general, a rapid decay in the downstream flow. Comparison with linear theory shows that the post-shock thermodynamic fluctuations in the region immediately behind the shock is mostly linear. The effect of upstream turbulent Mach number (or upstream turbulence intensity) is analyzed using the present simulations and available data from the literature. The post-shock field is found to be directly proportional with the upstream turbulent Mach number (M_t); monotonically increasing in amplitude behind the shock as upstream M_t is increased. Post-shock intensity of thermodynamic fluctuations were found to converge to the LIA limit as $M_t \to 0$ (or $M_t/[M-1] \to 0$). Finally, the effect of the shape of the energy spectrum in the upstream turbulent flowfield is analyzed, and is found to be significant in the rapidly decaying portion of the post-shock thermodynamic fluctuations.

1. Introduction

Shock waves are characteristic features in compressible flows, specifically in the supersonic/hypersonic flow regime. In aerospace applications, the effect of shock waves on the turbulent features in a supersonic boundary layer is usually studied to understand the physical mechanisms responsible for boundary layer separation, increased heat transfer and high surface pressures, each of which are unique engineering problems on their own. The interaction of free turbulence with a planar shock wave is a similar problem of interest, exhaustive with physical insights on the effects of shock on turbulence and vice-versa without additional complexities of mean shear, streamline curvature, wall effects, etc. Shock-turbulence interaction has implications in a variety of applications, to name a few, supersonic/hypersonic propulsion systems, inertial confinement fusion, shock wave lithotripsy, and in astrophysics (accretion shock waves). In this study, we focus on the interaction of a homogeneous isotropic turbulence interacting with a nominally planar shock wave, which is the most basic form of shock-turbulence interaction.

A brief but nearly complete information of the previous works, including recent experimental, theoretical and numerical studies on shock-turbulence interaction is provided

in [1] and in [2]. Compressible turbulent flows are characterized by the appreciable changes in thermodynamic quantities such as density, pressure and temperature fluctuations, which can be drastically amplified/altered/generated on interaction with shock waves. The importance of understanding the thermodynamic fluctuations is well known as they play a major role in turbulent mass flux, sound generation, turbulent heat flux, and most importantly, in the turbulent transport of energy between internal and kinetic energy components.

The objective of the present study is to perform a detailed investigation of the thermodynamic aspects of the canonical shock-turbulence interaction. This work attempts to explain the generation/amplification and evolution mechanisms of thermodynamic fluctuations in canonical shock-turbulence interaction by systematic variation of the governing parameters in the direct numerical simulations (DNS): flow Mach number (M), turbulent Mach number (M_t) and Taylor-scale Reynolds number (Re_λ). The physical mechanisms behind the variations in thermodynamic quantities are understood using LIA and the extensive DNS data of [3]. Additional numerical simulations have been carried out to supplement the existing data. A controlled study is carried out with purely vortical incoming turbulence in LIA and mostly vortical with minimal compressible fluctuations in the DNS data. The focus of this report is the effect of turbulent Mach number on the post-shock thermodynamic field.

2. Methodology

We use LIA and DNS to study the problem of a homogeneous isotropic turbulence (HIT), being convected by a uniform one-dimensional (1D) mean flow and interacting with a planar normal shock. Cartesian coordinate system is used where the shock-normal direction is represented by x and the shock-parallel directions by y and z. We use the notion of Favre (density-weighted) averages for all quantities except for density (ρ) and pressure (p), which follow Reynolds averaging. The Favre averages are denoted as $\widetilde{f}$ and the associated fluctuations are given by double primes whereas, the Reynolds averaged quantities denoted by an overbar and their respective fluctuations are denoted by single primes. When comparing results between LIA and DNS, we make use of the relation $\widetilde{f} \approx \overline{f}$ (linear limit), which is found to be valid everywhere in the domain except inside the region of the shock wave. The upstream and downstream states are denoted by subscripts 'u' and 'd' respectively.

2.1. *Numerical simulations*

An MPI based C++ code called 'Hybrid' [4] is used to solve the compressible Navier-Stokes equations for a perfect gas. The code uses a fifth-order WENO scheme with Roe flux-splitting around the shock and a sixth-order central scheme in the "split" form of [5] in the remainder of the domain. A shock wave is identified as the region where the negative dilatation is greater than the low pass-filtered vorticity magnitude, i.e., where $-\partial_{x_j} u_j > \sqrt{\omega_j \omega_j}$. The system of equations is integrated in time using a fourth-order accurate explicit Runge-Kutta scheme. This numerical procedure has been verified and validated on several problems of interest [3, 6, 7]. Further details about the code can be found in [3, 7].

The homogeneous/isotropic turbulence is generated as per the method given in [3] with the initial turbulent field specified using the von Kármán velocity spectrum having peak energy wavenumber of $k_0 = 4$. The isotropic databases are temporally decayed till

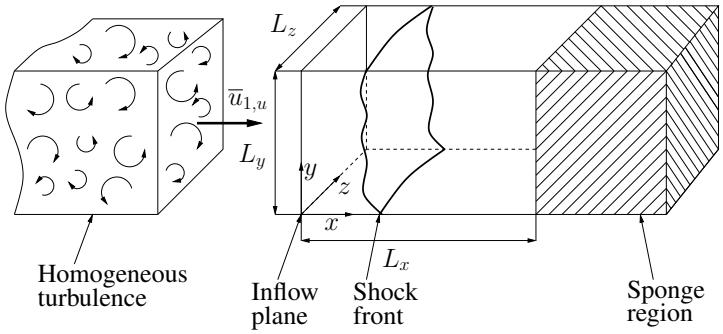

FIGURE 1. A schematic of the shock-turbulence interaction computational domain used in the numerical simulations

'realistic' turbulence is obtained, followed by a blending of multiple realizations to form a sufficiently long database that satisfies statistical convergence. Taylor's hypothesis is used to convect the blended database as the time-dependent inflow turbulence for the shock-turbulence interaction domain. The inflow turbulence used in the numerical simulations is quasi-vortical with minimal amount of thermodynamic and compressible fluctuations added using the method of [8]. The turbulence parameters immediately upstream of the shock are: turbulent Mach number $M_{t,u} = 0.15$, Taylor-scale Reynolds number of $Re_{\lambda,u} = 33$ and dissipation-scale Reynolds number $Re_{L_{\varepsilon,u}} \approx 135$.

Figure 1 shows the schematic of the computational domain with the shock-normal direction aligned with the streamwise direction (x). The computational domain is $k_0 L_x = 11\,\pi$ long in the streamwise direction with the shock initially placed at $k_0 x = 1\,\pi$, and is of length $k_0 L_y = k_0 L_z = 8\,\pi$ in each of the shock-parallel directions.

2.2. *Linear interaction analysis*

A single vorticity wave in two-dimensions (x, y) of amplitude A_v and at an angle ψ with the $x-$direction is being convected by a 1D uniform mean flow of velocity $\overline{u}_{1,u}$ towards the normal shock as shown in Fig. 2. The shock deforms in response and the position of the unsteady shock is given by $\xi(y,t)$. The downstream non-acoustic waves (entropy and vorticity) are generated/refracted at an angle $\overline{\psi}$ and are convected as 'frozen' waves by the downstream mean flow with velocity $\overline{u}_{1,d}$. The acoustic waves are generated at an angle $\widetilde{\psi}$ and are either propagating or decaying, depending on whether the angle of the incident wave is lower or higher than the critical angle.

The complete details of the LIA procedure can be obtained from [10], [2] and [11]. In brief, the linearized Euler equations are used to obtain the waveforms of the fluctuations in the upstream and downstream regions of the normal shock wave (modeled as a discontinuity). Linearized Rankine-Hugoniot conditions are used as the boundary conditions at the shock wave to obtain the transfer functions of the post-shock fluctuations. The upstream turbulence is represented as a super-position of 2D plane waves (Fourier modes), with each of them independently interacting with the shock. The post-shock field thus obtained is then integrated over all of the incident waves for a specified energy spectrum (von Kármán spectrum given in [12] is used here) to obtain a statistical description of the turbulence behind the shock wave. Therefore, we obtain

$$(\overline{f'_d g'_d})_{3D} = 4\pi \int_{k=0}^{\infty} \int_{\psi=0}^{\pi/2} (\overline{f'g'})_{2D}\, k^2\, \sin(\psi)\, d\psi\, dk \tag{2.1}$$

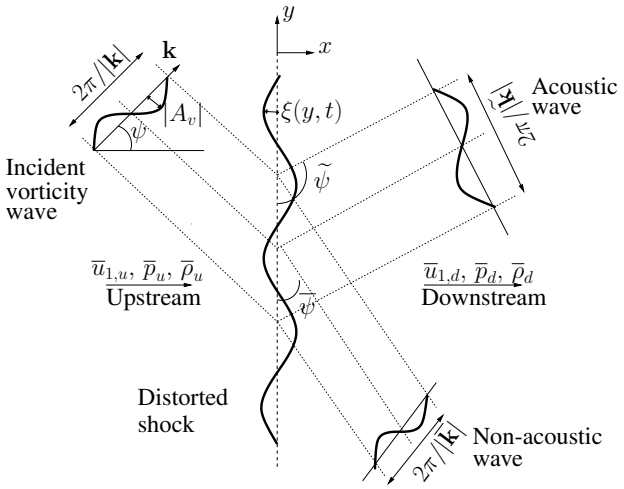

FIGURE 2. Linear interaction analysis framework to study the interaction of isotropic turbulence with a normal shock depicting the schematic of a single vorticity wave interacting with a normal shock (in 2D) and yielding three types of Kovásznay's linear waves [9].

where, $(\overline{f'_d g'_d})_{2D}$ is the correlation of the fluctuations f' and g' for a single wave of wavenumber k inclined at an angle of ψ.

The turbulence statistics are functions of the distance behind the shock wave, the Mach number of the upstream mean flow, and the incident turbulence energy spectrum. LIA predicts a jump in the turbulent fluctuations across the shock discontinuity, followed by an adjustment region. The inviscid adjustment is a result of the decaying acoustic energy corresponding to the elementary wave interactions with $\psi > \psi_c$, and is described in [2]. It is to be noted that the upstream turbulence considered in LIA is purely vortical with no thermodynamic fluctuations.

3. Simulation details

Simulations with four different upstream Mach numbers ($M_u = 1.23, 1.50, 2.50$ and 3.50) have been carried out in the present study. Additionally, the comprehensive statistics from the dataset of [3] with M_u ranging from 1.27 to 6 are also used when presenting the results. The present case details are tabulated in table 1. Along with the Taylor microscale Reynolds number, two other measures of the turbulence Reynolds number in the flowfield: the Reynolds number based on dissipation length scale (Re_{L_ϵ}) and the ratio of dissipation length scale (L_ϵ) to Kolmogrov length scale (η) are given in the fourth and fifth columns of the table.

M_u	$M_{t,u}$	$Re_{\lambda,u}$	$Re_{L_{\varepsilon,u}}$	$L_{\varepsilon,u}/\eta_u$	Grid
1.23	0.15	33	133	45	882×384^2
1.50	0.15	33	134	45	1042×384^2
2.50	0.15	33	135	46	1142×384^2
3.50	0.15	33	136	46	1313×384^2

TABLE 1. List of cases simulated in the present study

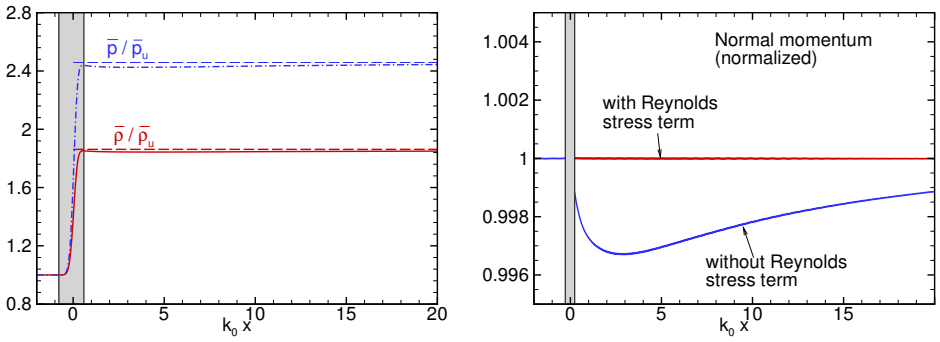

(a) Mean values of density and pressure (b) Mean of streamwise momentum

FIGURE 3. (a) Spatial variation of mean density (red solid) and pressure (blue dash-dotted) normalized by their respective mean values upstream of the shock. The dashed lines represent the inviscid jump values of density and pressure. (b) Spatial variation of mean streamwise momentum normalized by its respective upstream mean value with the shock-normal Reynolds stress (red) and without the Reynolds stress term (blue). The streamwise direction is normalized by the peak energy wavenumber. The region of unsteady shock movement is shown by the grey band.

3.1. *Conservation of mean quantities*

The numerical methodology used here captures the shock but the turbulence is adequately resolved. It is known that the Kolmogrov lengthscale decreases behind the shock [3]. The grid resolution is ensured to be sufficient enough to resolve the turbulence scales behind the shock (c.f. [13]). The normalized mean pressure and density are shown in Fig. 3(a) along with the inviscid jumps obtained using the Rankine-Hugoniot relations. There is a jump in the mean values at the shock, followed by a small decrease and a slow increase towards the outflow. This small decrease in mean values immediately behind the shock would lead one to believe that there is no conservation across the shock. In fact, this is due to the conservation of the mass, momentum and total enthalpy across the shock along with their respective turbulence terms. For example, consider the mean streamwise momentum equation where the quantity,

$$\overline{\rho}\widetilde{u}_1^2 + \overline{p} + [\overline{\rho}R_{11}] = const. \tag{3.1}$$

is to be conserved across the shock. The jump in streamwise Reynolds stress $[\overline{\rho}R_{11}]$ across the shock is the term due to turbulence which needs to be added to the laminar Rankine-Hugoniot conditions to ensure conservation. Figure 3(b) shows the variation of the sum of all terms in Eq. (3.1) with and without the Reynolds stress term. Neglecting the Reynolds stress term results in non-conservation behind the shock whereas, the inclusion of the Reynolds stress term ensures conservation. Thus, one can write the deviation in mean pressure (or density) from the inviscid Rankine-Hugoniot jumps as a function of the Reynolds stress terms, and can also see the deviation (or the small decrease) increase as upstream M_t is increased. We note that this slight change in the mean profiles however has a negligible impact on the turbulence.

3.2. *Normalization details*

We compare the thermodynamic variances ($\overline{\rho'^2}$, $\overline{p'^2}$, $\widetilde{T''^2}$, $\widetilde{s''^2}$) obtained from the DNS of canonical shock-turbulence interaction with the LIA predictions. We normalize the density, pressure and temperature variances by the square of their respective mean down-

stream values ($\overline{\rho}_d^2$, $\overline{p}_d^2$, $\widetilde{T}_d^2$). The entropy variance is normalized by the square of the gas specific heat capacity at constant pressure (c_p^2). Additionally, the variances are scaled by the upstream turbulent kinetic energy divided by the square of the upstream mean shock-normal velocity ($0.5\overline{u_{i,u}'^2}/\overline{u}_{1,u}^2$). This helps to compare different cases with varying upstream turbulence intensities. It also quantifies the conversion of upstream turbulent energy, primarily in the vortical component, into thermodynamic fluctuations by the shock wave. The streamwise coordinate is normalized by the peak energy wavenumber (k_0) in the upstream field. This normalization procedure is used throughout this report, unless otherwise specified.

3.3. *Data extraction*

Figure (4) shows the spatial variation of normalized streamwise Reynolds stress and pressure variance from DNS along with extrapolated values obtained by performing a linear least-squares fit over the DNS data from $x = x_{sp.} - 0.5\pi$. Here, $x_{sp.}$ denotes the start of the sponge region (or the end of the useful computational domain). This type of spatial extrapolation to the centre of the mean shock is used extensively in the literature, for example [3], [2], [14], when comparing far-field ($x \to \infty$) values between LIA and DNS. LIA provides an asymptotic value in the far-field region whereas, the DNS data shows a gradual decay due to viscous mechanisms. In DNS data, this procedure works well for velocity related quantities which have a non-monotonic variation behind the shock and for profiles with gradual variations such as entropy variances but fails to provide reasonable values for quantities having rapid variation behind the shock, for example the pressure variance. The spatial extrapolation method is not used in further analysis of the thermodynamic fluctuations due to this inadequacy.

Ideally, one would want to identify the actual far-field value by determining the location or estimating the multiple of lengthscale for the quantity of interest where there are minimal changes on the quantity (or the effect of source has disappeared). This is however difficult due to the limited size of the computational domain and the mixture of lengthscales in the post-shock turbulent flowfield. We, thus compare the solutions from LIA and DNS at selected locations instead of comparing far-field values.

4. Results and discussion

The effect of upstream flow Mach number on the thermodynamic fluctuations can be found in [13]. Budget of the terms in the transport equation of the thermodynamic fluctuations show that the dominant mechanism responsible for the convection of the thermodynamic fluctuations is the correlation of thermodynamic fluctuation with fluctuating dilatation [13]. We analyze the effect of upstream turbulent Mach number ($M_{t,u}$) on the thermodynamic fluctuations in this report. Additionally, the effect of the shape of the upstream turbulence energy spectrum is also discussed in this section.

4.1. *Effect of turbulent Mach number*

The generation of homogeneous isotropic turbulence databases in the DNS warrants special attention when the effect of turbulent Mach number is analyzed. The initial turbulent field in the triply periodic box is isotropic and solenoidal in nature with an energy spectrum specified in the form of von Kármán energy spectrum [12]. The pressure fluctuations are not independent of the velocity field but are set by the solenoidal velocity fluctuations via the ‘pseudo-pressure’ relationship which in turn also affects the density

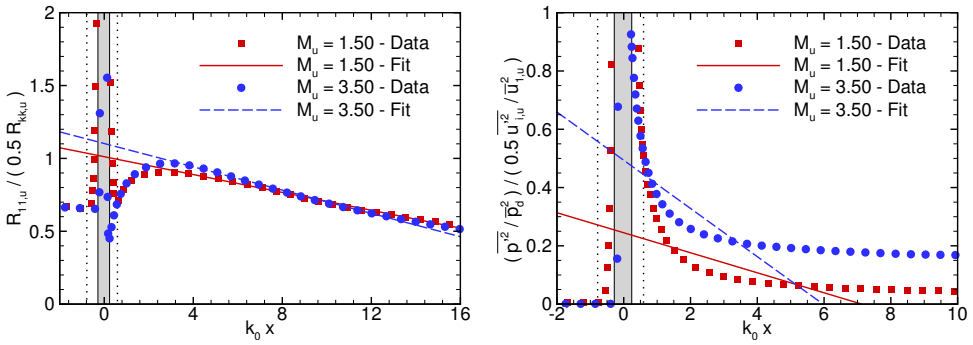

(a) Normalized shock-normal Reynolds stress (b) Normalized pressure variance

FIGURE 4. Spatial variation of (a) normalized shock-normal Reynolds stress, (b) normalized pressure variances for the cases of $M_u = 1.50$ and 3.50 with $M_{t,u} = 0.15$ and $Re_{\lambda,u} = 33$. The Reynolds stress term is normalized by the upstream turbulent kinetic energy (TKE) and the pressure variance is normalized as mentioned in Sec. 3.2. The data is shown by symbols and the lines represent the linear least-squares fit to the data from the end of the useful computational domain. The grey band shows the region of unsteady shock movement for $M_u = 3.50$ and the vertical dotted lines correspond to that of the $M_u = 1.50$ case.

and temperature fluctuations via the adiabatic relations [8]. The pressure fluctuations are related to the initial solenoidal velocity field as,

$$p' \sim \overline{\rho} u_i'^2, \quad \frac{p'}{\overline{p}} \sim \gamma M_t^2, \tag{4.1}$$

and is obtained by solving a pressure Poisson equation. The thermodynamic quantities are related to each other via the linearized adiabatic relations as,

$$\frac{\rho'}{\overline{\rho}} = \frac{p'}{\gamma \overline{p}} = \frac{T'}{(\gamma - 1)\overline{T}} \tag{4.2}$$

The amplitude of the thermodynamic field is thus directly proportional to the square of the turbulent Mach number in the database and increases as the turbulent Mach number is increased. Additionally, small amount of pressure and dilatation fluctuations are added as a result of the blending procedure. Blending of multiple isotropic boxes is carried out to obtain a long database in time for statistical convergence. Large amount of dilatational fluctuations are added as a result of using Taylor's hypothesis to convect the turbulent flowfield in the shock-turbulence interaction domain. This is due to the inapplicability of Taylor's hypothesis for the acoustic waves present in compressible turbulence. Nonetheless, the energy of the compressible fluctuations in the turbulence database is very small (about $1 - 2\%$ of the total energy) in comparison to the energy present in the solenoidal velocity fluctuations. The upstream region in the shock-turbulence interaction domain thus have finite values of thermodynamic fluctuations and they also contribute to the post-shock thermodynamic fluctuations.

Figure 5 shows the spatial variation of the normalized thermodynamic variances from DNS for the case of $M_u = 1.50$ and $Re_{\lambda,u} = 40$ available in [3]. The corresponding LIA solution obtained for $M_u = 1.50$ is also plotted for comparison. All the variances show a large jump inside the shock followed by a rapid decay except the entropy variance which decays gradually behind the shock. As expected, the DNS values converge to the LIA solution as $M_{t,u} \to 0$. The post-shock intensity of the thermodynamic fluctuations

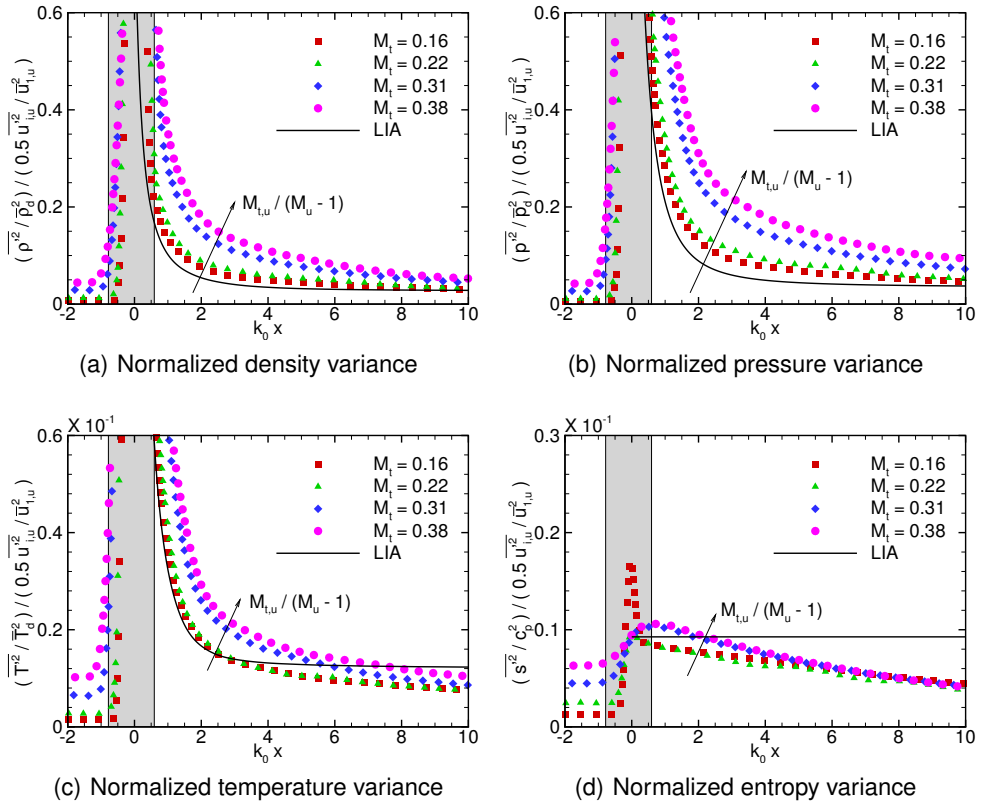

(a) Normalized density variance (b) Normalized pressure variance

(c) Normalized temperature variance (d) Normalized entropy variance

FIGURE 5. Spatial variation of normalized thermodynamic variances for varying $M_{t,u}$ values from the dataset of $M_u = 1.50$ and $Re_{\lambda,u} = 40$. The normalization is as mentioned in Sec. 3.2. The symbols represent DNS solutions and the line corresponds to the LIA solution. The grey band shows the region of unsteady shock movement.

increase proportionally to the increase in the upstream turbulent Mach number. The numerical shock thickness also varies proportionally to $M_{t,u}$ with the shock being thicker for high $M_{t,u}$ values. The LIA solution asymptote to a constant value beyond $k_0 x \geq 6$ whereas, the DNS solution decays due to the viscous mechanisms. There is a good match between the LIA and DNS solutions in the region immediately behind the shock (rapidly decaying region) which is found to be dominated by the acoustic mode for low Mach numbers. Further downstream, the effect of entropy mode becomes dominant and large deviations between DNS and LIA solutions are observed as a result of the viscous effects.

Figure 6 compare the normalized thermodynamic variances from DNS ($Re_{\lambda,u} = 40$) to that of the solution obtained from LIA at the location $k_0 x = 0.25\pi$ for varying upstream turbulent Mach numbers and flow Mach numbers. Large values are found for the high Mach number cases and the simultaneous effect of the increasing turbulent Mach number is also observed. Temperature and entropy variances for low Mach numbers are very small in intensity compared to their density and pressure counterparts but are comparable at high Mach numbers. The few outliers in the DNS data are assumed to be due to numerical errors/insufficient resolution in the simulations. Interestingly, the DNS values are larger than the LIA solutions at this location for low Mach numbers but are

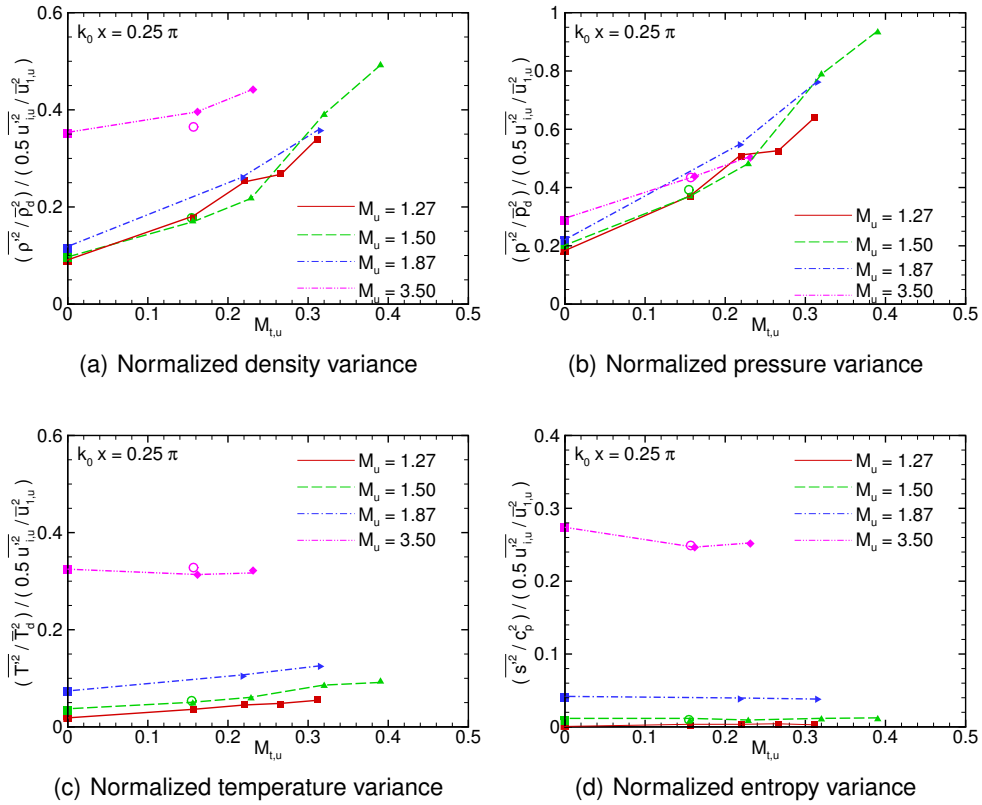

FIGURE 6. Variation of normalized thermodynamic variances against $M_{t,u}$ from the dataset of $Re_{\lambda,u} = 40$ and $M_u = 1.27$ (red squares), 1.50 (green delta), 1.87 (blue right triangles), 3.50 (pink diamonds). The solutions from present simulations are shown by hollow circles: $M_u = 1.50$ (green) and 3.50 (pink). The squares at $M_t = 0$ correspond to the LIA solution for the respective Mach numbers indicated by the colors. The normalization is as mentioned in Sec. 3.2.

comparable in values to the high Mach number cases. This is entirely due to the choice of a constant location which falls marginally at the downstream edge of the unsteady shock region for the low Mach number cases but is outside for the high Mach number case. The relatively higher values in the DNS for the $M_u = 3.50$ case is hypothesized to be an artefact of the differences in upstream turbulence energy spectrum, and will be discussed in Sec. 4.2.

The normalized thermodynamic variances from DNS and LIA at the location $k_0x = 2\pi$ is shown in Fig. 7. The intensity of the variances is low compared to the values obtained at the location $k_0x = 0.25\pi$ except for the LIA value of entropy variance which remains constant at all locations. As expected, the DNS values have decreased by factor of 2 or more and there are only very small changes in the LIA solution. The DNS values for the thermodynamic variances are larger than the LIA solutions for low Mach numbers having high $M_{t,u}$ values and are lower than LIA values for low $M_{t,u}$ values for the same upstream flow Mach number. Once again, as the $M_{t,u}$ value is reduced, the DNS solution converges to the LIA limit.

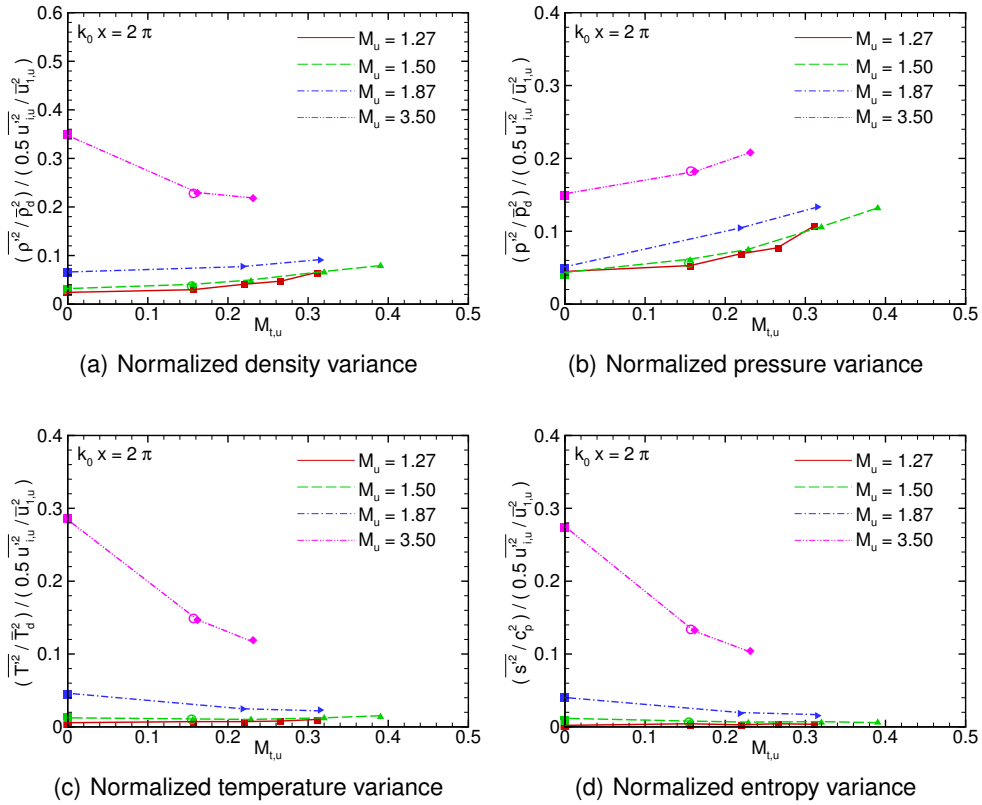

(a) Normalized density variance (b) Normalized pressure variance

(c) Normalized temperature variance (d) Normalized entropy variance

FIGURE 7. Spatial variation of normalized thermodynamic variances for varying $M_{t,u}$ values from the dataset of $M_u = 1.50$ and $Re_{\lambda,u} = 40$. The color legend is the same as mentioned in caption of Fig. 6. The normalization is as mentioned in Sec. 3.2.

4.2. *Effect of upstream turbulence shape*

The effect of the shape of the upstream turbulence spectrum is analyzed in Fig. 8 by comparing the thermodynamic variances for two different turbulence spectrum. The spectra used in this analysis are the exponential spectrum given by the expression,

$$E(k) \sim (k/k_0)^4 \, e^{-2(k/k_0)^2} \tag{4.3}$$

and the von Kármán spectrum [12], which is expressed as,

$$E(k) \sim \frac{(k/k_0)^2}{\left[(k/k_0)^2 + (5/6)\right]^{11/6}} \tag{4.4}$$

The variances are found to be independent at the locations immediately behind the shock ($x = 0^+$) and at the far-field ($x \to \infty$). In the rapidly decaying region ($0.25 < k_0 x < 2$), there are significant variations between results from the two spectrum shapes, specifically in the location and intensity of the post-shock peak observed in the density variance. The von Kármán spectrum matches better in comparison to the exponential spectrum since the initial spectrum in the DNS cases were also of the former type. There are still variations between LIA and DNS results, especially in the pressure fluctuations

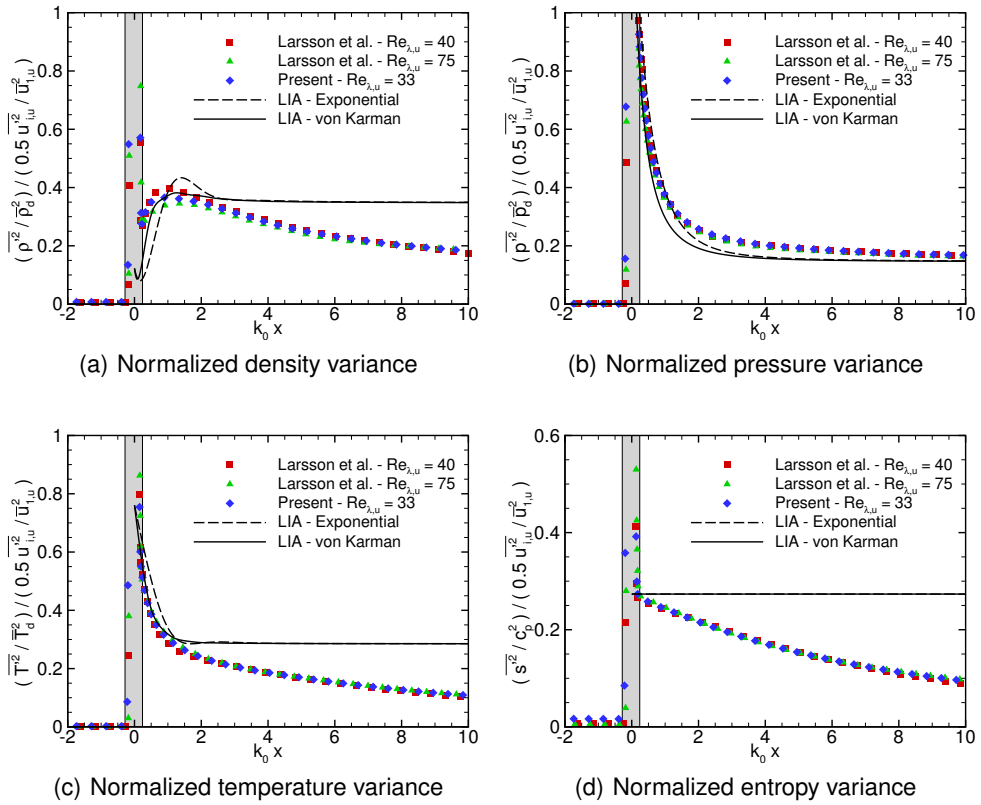

(a) Normalized density variance (b) Normalized pressure variance

(c) Normalized temperature variance (d) Normalized entropy variance

FIGURE 8. Spatial variation of normalized thermodynamic variances from the dataset of $M_u = 3.50$, $M_{t,u} = (0.15, 0.16)$ and $Re_{\lambda,u} = (33, 40, 75)$. The normalization followed is as mentioned in Sec. 3.2. Symbols correspond to DNS data and the lines represent LIA solutions obtained using two different turbulence energy spectrum. The region of unsteady shock movement is shown by a grey band.

which implies that an exact match is possible only when the same energy spectrum used in the DNS is also applied in LIA. This was also verified in the work of [11] where the inflow turbulence from DNS is applied in LIA to obtain reliable post-shock flowfields for high Reynolds numbers, which are in general difficult to obtain using DNS.

The effect of upstream turbulence Reynolds number based on Taylor microscale is found to be negligible on the thermodynamic fluctuations. It has been reported in [3] that the Reynolds stresses are closer to the LIA values at high Reynolds numbers compared to the low Reynolds number cases. [14] also report a similar trend for the heat flux correlation approaching the LIA values as the turbulence Reynolds number is increased. Velocity fluctuations and its related correlations with other quantities are found to be significantly affected by the variations in turbulence Reynolds number however, no such definite conclusions cannot be drawn for the thermodynamic fluctuations with the available sparse data (in terms of Re_λ).

5. Conclusion

In this work, we presented a comparison of the thermodynamic fluctuations generated by canonical shock-turbulence interaction between LIA and DNS. A large parameter space including a range of Mach number, turbulent Mach number and Reynolds number is considered, and available DNS data is complemented with new cases computed here.

The effect of turbulent Mach number on the thermodynamic fluctuations is analyzed. Large values of thermodynamic fluctuations are found in the upstream region as turbulent Mach number is increased. This is due to the methodology by which compressible fluctuations are added to the pre-shock turbulence. The post-shock thermodynamic fluctuations were also found to be amplified across the shock for increasing $M_{t,u}$ values proportional to the shock strength. The finite values of upstream thermodynamic fluctuations contribute to the intensity of the post-shock thermodynamic fluctuations generated/amplified by the shock. It was found that the thermodynamic fluctuations converge to the LIA limit as the upstream turbulent Mach number (or the upstream turbulence intensity) is reduced.

The shape of the turbulence energy spectrum is found to have a significant effect in the rapidly varying portion of the thermodynamic field behind the shock. The spectrum shape, however is found to have no effect immediately behind the shock ($x = 0^+$) and at the far-field location ($x = \infty$). The effect of Taylor scale Reynolds number on the thermodynamic field is found to be minimal with the available data, and requires further data for a much wider range of Reynolds numbers to provide definite conclusions.

Acknowledgments

Financial support has been provided by the German Research Foundation (Deutsche Forschungsgemeinschaft – DFG) in the framework of the Sonderforschungsbereich Transregio 40. Computational support was provided by the LRZ:Leibniz Research Centre, Munich, Germany as part of the SFB TRR40 Summer Program 2017 and by the NPSF Param YUVA-II supercomputing facility, C-DAC, Pune, India. The authors thank the external collaborator, Dr. Johan Larsson of the University of Maryland for the numerical code, many discussions and the comprehensive DNS statistics.

References

[1] KITAMURA, T., NAGATA, K., SAKAI, Y., SASOH, A. AND ITO, Y. (2016). Rapid distortion theory analysis on the interaction between homogeneous turbulence and a planar shock wave. *J. Fluid Mech.*, **802**, 108 – 146.

[2] QUADROS, R., SINHA, K. AND LARSSON, J. (2016). Turbulent energy flux generated by shock/homogeneous-turbulence interaction. *J. Fluid Mech.*, **796**, 113 – 157.

[3] LARSSON, J., BERMEJO-MORENO, I. AND LELE, S.K. (2013). Reynolds-and Mach-number effects in canonical shock-turbulence interaction. *J. Fluid Mech.*, **717**, 293 – 321.

[4] BERMEJO-MORENO, I., BODART, J., LARSSON, J., BARNEY, B.M., NICHOLS, J.W. AND JONES, S. (2013). Solving the compressible navier-stokes equations on up to 1.97 million cores and 4.1 trillion grid points. In: *Proc. Int. Conf. High Perform. Comput. Networking, Storage Anal.* SC '13, ACM, New York, NY, USA, 62:1 – 62:10.

[5] DUCROS, F., LAPORTE, F., SOULÈRES, T., GUINOT, V., MOINAT, P. AND CARUELLE, B. (2000). High-Order Fluxes for Conservative Skew-Symmetric-like Schemes in Structured Meshes: Application to Compressible Flows. *J. Comput. Phys.*, **161**(1), 114 – 139.

[6] JOHNSEN, E., LARSSON, J., BHAGATWALA, A.V., CABOT, W.H., MOIN, P., OLSON, B.J., RAWAT, P.S., SHANKAR, S.K., SJÖGREEN, B., YEE, H.C., ZHONG, X. AND LELE, S.K. (2010). Assessment of high-resolution methods for numerical simulations of compressible turbulence with shock waves. *J. Comput. Phys.*, **229**(4), 1213 – 1237.

[7] LARSSON, J. AND LELE, S.K. (2009). Direct numerical simulation of canonical shock/turbulence interaction. *Phys. Fluids*, **21**(12), 126101.

[8] RISTORCELLI, J.R. AND BLAISDELL, G.A. (1997). Consistent initial conditions for the DNS of compressible turbulence. *Phys. Fluids*, **9**(1), 4 – 6.

[9] KOVÁSZNAY, L.S.G. (1953). Turbulence in Supersonic Flow. *J. Aeronaut. Sci.*, **20**(10), 657 – 674, 682. Reprinted in *AIAA J.*, **41(7)**, 219-237, 2003.

[10] MAHESH, K., MOIN, P. AND LELE, S.K. (1996). *The interaction of a shock wave with a turbulent shear flow*. Tech. Rep. TF-69, Thermosciences Division, Department of Mechanical Engineering, Stanford University, Stanford, California 94305.

[11] LIVESCU, D. AND RYU, J. (2016). Vorticity dynamics after the shock-turbulence interaction. *Shock Waves*, **26**(3), 241 – 251.

[12] LARSSON, J. (2010). Effect of Shock-Capturing Errors on Turbulence Statistics. *AIAA J.*, **48**(7), 1554 – 1557.

[13] YOGESH PRASAAD, M.S., SINHA, K. AND LARSSON, J. (2017). Thermodynamic Fluctuations In Canonical Shock-turbulence Interaction. In: *Proc. Tenth Int. Symp. on Turbul. and Shear Flow Phenom.* TSFP10, 8C–4:1 – 8C–4:6. URL {http://www.tsfp-conference.org/proceedings/tsfp10-contents-of-volume-3.html}.

[14] QUADROS, R., SINHA, K. AND LARSSON, J. (2016). Kovasznay Mode Decomposition of Velocity-Temperature Correlation in Canonical Shock-Turbulence Interaction. *Flow, Turbul. and Combust.*, **97**(3), 787 – 810.